Numerical exploration of non-axisymmetric divertor closure in the small angle slot (SAS) divertor at DIII-D

H. Frerichs,[1] O. Schmitz,[1] B. Covele,[2] Y. Feng,[3] H.Y. Guo,[2] and D. Hill[2]
[1)] *University of Wisconsin - Madison, Department of Engineering Physics, Madison, WI 53706, USA*
[2)] *General Atomics, San Diego, CA 92186, USA*
[3)] *Max-Planck Institute for Plasma Physics, Greifswald, Germany*

(Dated: 14 November 2017)

Numerical simulations of toroidal asymmetries in a tightly baffled small angle slot (SAS) divertor on the DIII-D tokamak show that toroidal asymmetries in divertor closure result in (non-axisymmetric) local onset of detachment within a density window of $10-15\,\%$ on top of the nominal threshold separatrix density. The SAS divertor is explored at DIII-D for improving access to cold, dissipative/detached divertor conditions. The narrow width of the slot divertor coupled with a small magnetic field line-to-target angle facilitates the buildup of neutral density, thereby increasing radiative and neutrals-related (atoms and molecules) losses in the divertor. Small changes in the strike point location can be expected to have a large impact on divertor conditions. The combination of misaligned slot structure and non-axisymmetric perturbations to the magnetic field configuration causes the strike point to move along the divertor target plate, possibly leaving the divertor slot at some locations. The latter extreme case essentially introduces an opening in the divertor slot from where recycling neutrals can easily escape, and thereby degrade the performance of the slot divertor. Such a strike point dislocation is approximated by a finite gap in the divertor baffle for which three dimensional edge plasma and neutral gas simulations are performed with the EMC3-EIRENE code.

The control of heat loads remains a key challenge for the development and operation of fusion reactors as well as for the next-step fusion device ITER[1]. This is because present materials for plasma facing components require heat flux densities of the order $q_t \leq 10\,\mathrm{MW\,m^{-2}}$, as well as low temperatures $T_e \leq 5\,\mathrm{eV}$ to suppress erosion[2] for an adequate lifetime. Increased divertor closure is found to be beneficial for energy dissipation related to the buildup of neutral density[3], and this facilitates onset of detachment at lower main plasma density. Following experiments on divertor closure at ASDEX Upgrade, JET[4] and Alcator C-mod[5], a new divertor configuration is implemented in DIII-D: the small angle slot (SAS) divertor[6,7] which aims at improving the understanding of divertor closure effects on detachment. Design and optimization of the SAS divertor has been carried out with the two-dimensional (2D) scrape-off layer plasma simulation (SOLPS) code[8], which has played a key role in designing the ITER divertor as well[9].

While the narrow slot of the SAS divertor increases divertor closure, divertor operation can be expected to be more sensitive to small changes in the strike point location. The combination of misaligned slot structure and non-axisymmetric perturbations to the magnetic field configuration (either intentionally by external coils for the control of ELMs, or unintentionally due to coil misalignments) causes the strike point to move along the divertor target plate, possibly leaving the divertor slot at some locations. Consequently, divertor closure is reduced and recycling neutral particles can escape more easily, degrading the performance of the slot divertor.

In the present letter we explore such a toroidally localized change in divertor closure, which is motivated by the presence of an error field from the field coils and a small misalignment between the center stack and the divertor slot. For the initial assessment here, we approximate this misalignment by a finite gap in the divertor baffle. We choose the size of the gap to be $\Delta\varphi = 20$ deg (which corresponds to approx. 50 cm), and apply a flat continuation of the main divertor plate within the gap (see figure 1). Moreover, we choose 3 symmetric gaps to facilitate $n = 3$ toroidal symmetry in order to reduce the computational load. This approximation does not require detailed knowledge about the error fields and the alignment of the divertor baffle components, but can still provide insight into the general trends related to a local degra-

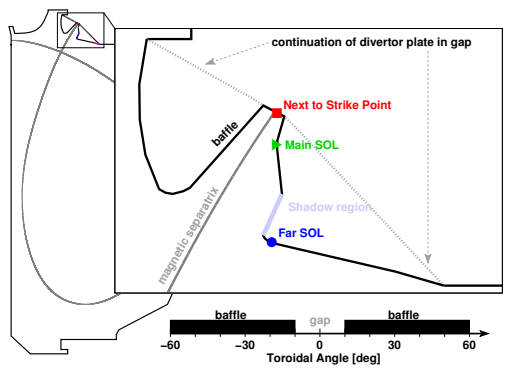

FIG. 1. The SAS divertor configuration in DIII-D. Misalignment between the strike point and the divertor slot is approximated by a finite toroidal gap in the divertor baffle at $\varphi = -10 \ldots 10$ deg. A flat continuation of the main divertor plate is applied within the gap (dashed line).

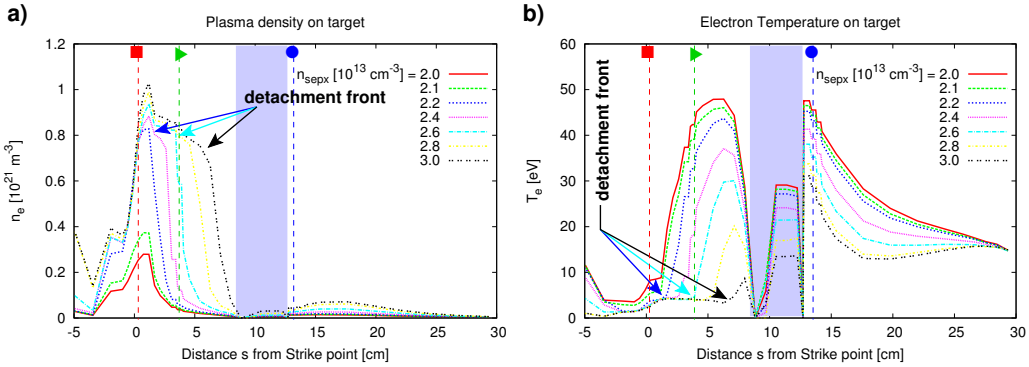

FIG. 2. Reference profiles along the SAS divertor target from an axisymmetric configuration: (a) plasma density n and (b) electron temperature T_e. The highlighted points next to the strike point and in the SOL correspond to the points of the same color and style on the divertor outline in figure 1.

dation of the divertor closure. This extreme case does not necessarily reflect a realistic configuration at DIII-D, but should rather be seen as a motivation for subsequent more elaborate simulations. It does, however, provide a first estimate of the impact of a toroidally localized loss of divertor closure.

The magnetic configuration in our simulations has been modelled by EFIT[10] in preparation for the upcoming SAS experiments. An upper single null configuration with plasma current $I_p = 1\,\mathrm{MA}$ and toroidal magnetic field of $B_t = 2\,\mathrm{T}$ at the magnetic axis is used. Its shape is characterized by an elongation of $\kappa = 1.7$, and an upper and lower triangularity of $\delta_u = 0.51$ and $\delta_l = 0.22$, respectively. Three-dimensional (3D) modeling of the boundary plasma is performed with the EMC3-EIRENE package[11,12]. The EMC3 model applies a fluid approach for the main plasma species (deuterium) and trace impurities (carbon), while interactions with neutral gas are calculated by EIRENE. Iterating between edge plasma and neutral gas solver provides a self-consistent, steady state solution. Anomalous cross field transport is taken into account by model parameters, which have been set to $D_\perp = 0.5\,\mathrm{m^2\,s^{-1}}$ and $\chi_{\perp,e} = \chi_{\perp,i} = 1.5\,\mathrm{m^2\,s^{-1}}$. These coefficients are constant throughout the simulation domain in the present exploratory study, but they have been chosen from the range of radially varying coefficients from $D_\perp = 0.1 - 0.3\,\mathrm{m^2\,s^{-1}}$ around the separatrix to $D_\perp = 1\,\mathrm{m^2\,s^{-1}}$ in the far SOL as used in SOLPS simulations for DIII-D[6,13]. Cross-field drifts (mainly $E \times B$ and diamagnetic drifts) are not yet implemented in EMC3-EIRENE, but those are also switched off in corresponding SOLPS modeling[6,7]. Divertor pumping has been implemented in EMC3-EIRENE[14], but is not switched on for the present exploratory study (as in corresponding SOLPS modeling[6,7]). This represents an upper limit to the leakage introduced by the gap as pumping will decrease the D_2 density in the slot as well. Perturbations to the main plasma species are due to the cooling of the electrons only in the trace impurity approximation. The present simulations include carbon as the only impurity species for which the same temperature as the main ions is assumed. Carbon production is due to the impinging deuterium ions with an overall (chemical and physical) sputter yield of $Y = 4\,\%$. While this is on the upper end of reasonable values for sputtering, its main impact here is providing local power losses for electrons from radiation, and these are usually underestimated in modeling[13,15]. The inner simulation boundary for the plasma edge is set at $\Psi_N = 0.99$ normalized poloidal flux with an additional core domain for neutral particles. Core particle fueling is set to $80\,\mathrm{A}$ (on top of a self-consistent contribution from recycling neutral particles that are ionized in the core), and the flux surface averaged density just inside the separatrix n_{sepx} is used as a control parameter which determines the recycling flux. The edge input power of $P_{\mathrm{in}} = 4\,\mathrm{MW}$ is split equally between electrons and ions.

First, a density scan for the axisymmetric configuration has been performed to set up a reference. The separatrix density is increased from $n_{\mathrm{sepx}} = 2.0 \cdot 10^{19}\,\mathrm{m^{-3}}$ to $3.0 \cdot 10^{19}\,\mathrm{m^{-3}}$ in 10 steps. The plasma is still attached at the lowest density, and continuously detaches along the divertor target with increasing density. In the following we take $T_e \leq 4\,\mathrm{eV}$ as necessary condition for local detachment which is when momentum losses due to ion-neutral collisions (charge exchange) become relevant. Profiles of the electron density and temperature along the SAS divertor target are shown in figure 2 where $s = 0$ refers to the location of the separatrix strike point. It can be seen that the density around the strike point (red square in figure 1) significantly increases between $n_{\mathrm{sepx}} = 2.1 \cdot 10^{19}\,\mathrm{m^{-3}}$ and $2.2 \cdot 10^{19}\,\mathrm{m^{-3}}$ with a corresponding drop in temperature to $4\,\mathrm{eV}$. This is the onset of partial detachment at the strike point where the temperature along the side segments of the divertor slot remains above this threshold for detachment. The extent

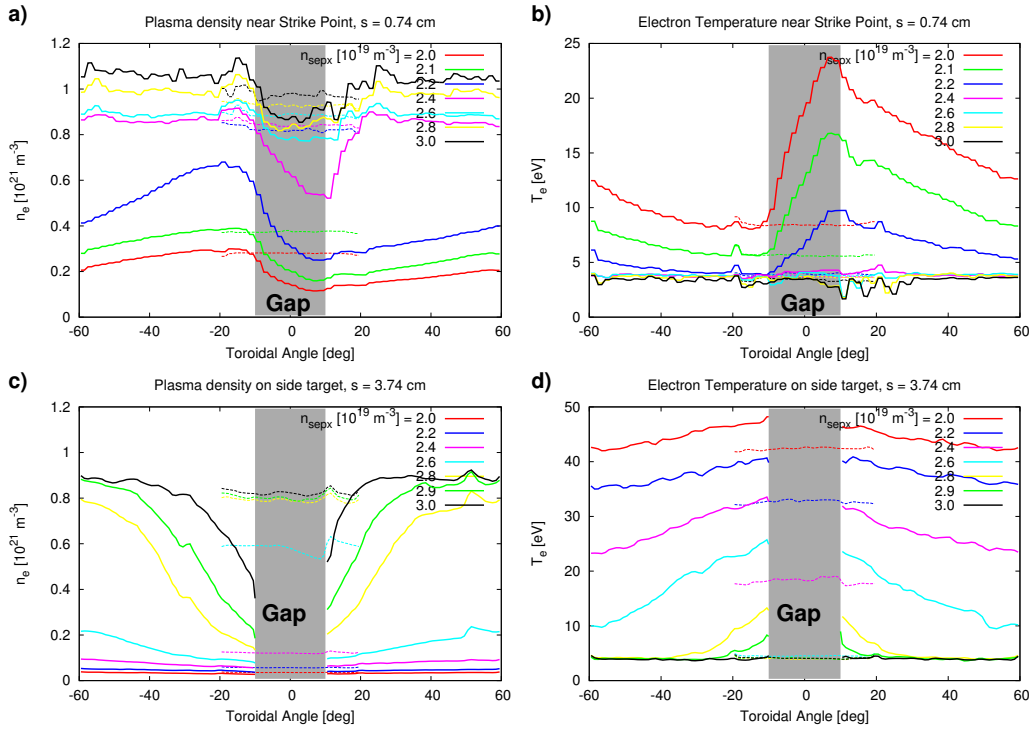

FIG. 3. Toroidal profiles of divertor density and temperature: (a,b) next to the separatrix strike point at $s = 0.74\,\mathrm{cm}$ (red squre in figure 1), and (c,d) further along the side of the divertor target at $s = 3.74\,\mathrm{cm}$ in the main SOL (green triangle in figure 1). The dashed lines indicate the reference values for the different separatrix densities as shown in the same color (note that a 40 deg sub-block has been chosen for the simulation domain for the axisymmetric reference cases).

of partial detachment can be characterized by the location of the detachment front s_{detach} along the target, i.e. the location where T_e drops below 4 eV with a significant increase of n_e.

After the onset of detachment at the strike point, gradually increasing the separatrix density from $2.2 \cdot 10^{19}\,\mathrm{m}^{-3}$ to $3.0 \cdot 10^{19}\,\mathrm{m}^{-3}$ results only in a moderate further increase of density at the strike point itself. On the other hand, the extent of the high density zone in the divertor slot grows along the target with increasing n_{sepx}. It can be seen in figure 2 that the detachment front s_{detach} moves along the side segments of the divertor slot from $s_{\mathrm{detach}} \approx 1\,\mathrm{cm}$ at $n_{\mathrm{sepx}} = 2.2 \cdot 10^{19}\,\mathrm{m}^{-3}$ to $s_{\mathrm{detach}} \approx 7\,\mathrm{cm}$ at $n_{\mathrm{sepx}} = 3.0 \cdot 10^{19}\,\mathrm{m}^{-3}$. The outermost part of the divertor slot (light blue segment in figure 1) is located in the shadow region of the flux surface that just passes the edge of the slot.

In the following we explore the impact of a toroidally localized loss of divertor closure. The same density scan is performed for a configuration with a gap in the divertor baffle as depicted in figure 1. While the divertor slot facilitates the buildup of neutral gas, a gap in the baffle leads to a local loss of neutral particles and related recycling. Consequently, the divertor density will be reduced. The toroidal dependence of this effect is summarized in figure 3. Field lines intersect the SAS divertor target in forward toroidal direction, i.e. going from left to right in figure 3. It can be seen in figure 3 (a) that the maximum divertor density is achieved at $\varphi = -20 \ldots -10$ deg, i.e. just before field lines go through the gap region. At lowest separatrix density (attached case, red), the divertor density near the strike point drops by a factor of 2 in the gap with respect to the no-gap reference case (dashed lines). This loss of divertor density takes about $\Delta\varphi = 80$ deg to recover to the reference value.

The onset of partial detachment in the no-gap reference case occurs at $n_{\mathrm{sepx}} = 2.2 \cdot 10^{19}\,\mathrm{m}^{-3}$. It can be seen in figure 3 (b) that the loss of divertor density in the gap results in a local increase of divertor temperature. In particular, it can be seen that the threshold n_{sepx} for onset of detachment is locally raised: at $n_{\mathrm{sepx}} = 2.2 \cdot 10^{19}\,\mathrm{m}^{-3}$ (blue profiles), the divertor temperature is raised to about 10 eV at the downstream end of the gap, and remains above 5 eV for more than 50 deg toroidally, i.e. the plasma remains attached for a significant distance in toroidal direction. Nevertheless, at

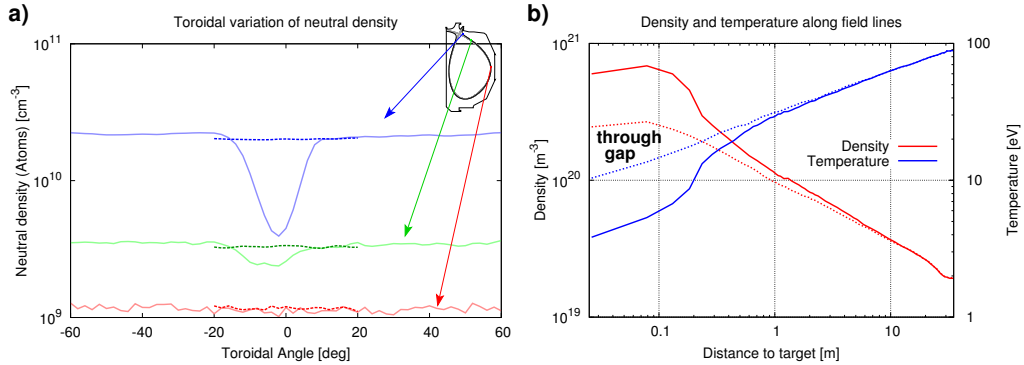

FIG. 4. (a) Toroidal profiles of the atomic hydrogen density at three locations between the X-points and the midplane, dashed lines represent the no-gap reference case. (b) Density and temperature profiles along field lines at $n_{\mathrm{sepx}} = 2.2 \cdot 10^{19}\,\mathrm{m}^{-3}$: connecting to the target through the gap at $\varphi = 11$ deg (dashed lines) and connecting to the target just before the gap at $\varphi = -11$ deg (solid lines).

higher n_{sepx}, loss of divertor density is recovered within a shorter toroidal distance from the gap, and detachment near the strike point can be maintained already at $n_{\mathrm{sepx}} = 2.4 \cdot 10^{19}\,\mathrm{m}^{-3}$ throughout the toroidal direction.

Higher n_{sepx} is required for transition to detachment further along the divertor target in the main SOL. At only a few cm from the strike point location (i.e. at the green triangle in figure 1), the threshold density is $n_{\mathrm{sepx}} = 2.6 \cdot 10^{19}\,\mathrm{m}^{-3}$ in the no-gap reference case. It can be seen in figures 3 (c) and (d) that at this n_{sepx} (cyan profiles), the gap results in a significant reduction of divertor density throughout the entire toroidal direction. Consequently, the local divertor temperature increases to 25 eV at the edges of the gap, and to 10 eV at the toroidal location farthest away from the gap. Thus, this location remains fully attached at this n_{sepx}. Further increase of n_{sepx} recovers partial detachment in toroidal direction, and toroidally homogeneous detachment is recovered at $n_{\mathrm{sepx}} = 3.0 \cdot 10^{19}\,\mathrm{m}^{-3}$.

Conversely, the non-axisymmetric divertor conditions have little to no impact on upstream conditions. Toroidal profiles of the atomic hydrogen density are shown in figure 4 (a). While the neutral density near the X-point is significantly affected by the gap, only a small impact is found on the same flux surface $\Delta Z = -20\,\mathrm{cm}$ below the X-point, and axisymmetric conditions are recovered upstream at the midplane (i.e. neutral particles have travelled far enough to smooth out their toroidally inhomogeneous source). Homogeneous plasma conditions upstream are confirmed for two field lines in figure 4 (b): one connects to the target going through the gap, and the other connects to the target just before the gap. It can be seen that upstream densities and temperatures are identical on both field lines. Downstream, however, the field line that does not go through the gap profits from a buildup of neutral density (and consequently plasma density) inside the narrow divertor slot, and this results in lower temperatures required for detachment.

In summary, simulations show that a toroidally localized loss of divertor closure (here explored by a gap in the baffle) raises the midplane density threshold for detachment by a small amount. The loss of recycled neutral particles in the gap results in toroidally localized lower divertor densities at which the plasma remains attached. Conversely, it can detach at toroidal locations less affected by the gap at the same upstream conditions. Nevertheless, toroidally homogeneous detachment can still be achieved at somewhat higher $(10 - 15\,\%)$ separatrix densities.

ACKNOWLEDGEMENTS

This work has been funded in part by the U.S. Department of Energy under DE-SC0013911 and DE-FC02-04ER54698. DIII-D data shown in this paper can be obtained in digital format by following the links at https://fusion.gat.com/global/D3D DMP.

REFERENCES

[1] A. Loarte, B. Lipschultz, A. S. Kukushkin, G. F. Matthews, P. C. Stangeby, N. Asakura, G. F. Counsell, G. Federici, A. Kallenbach, K. Krieger, A. Mahdavi, V. Philipps, D. Reiter, J. Roth, J. Strachan, D. Whyte, R. Doerner, T. Eich, W. Fundamenski, A. Herrmann, M. Fenstermacher, P. Ghendrih, M. Groth, A. Kirschner, S. Konoshima, B. LaBombard, P. Lang, A. W. Leonard, P. Monier-Garbet, R. Neu, H. Pacher, B. Pegourie, R. A. Pitts, S. Takamura, J. Terry, E. Tsitrone, and the ITPA Scrape-off Layer and Divertor Physics Topical Group. Chapter 4: Power and particle control. *Nuclear Fusion*, 47:S203–S263, 2007.

[2] P.C. Stangeby and A.W. Leonard. Obtaining reactor-relevant divertor conditions in tokamaks. *Nuclear Fusion*, 51:063001, 2011.

[3] A. Loarte. Effects of divertor geometry on tokamak plasmas. *Plasma Phys. Control. Fusion*, 43:R183, 2001.

[4] A. Kallenbach, D. Coster nad J. C. Fuchs, H. Y. Guo, G. Haas, A. Herrmann, L. D. Horton, L. C. Ingesson, C. F. Maggi, G. F. Matthews, R. D. Monk, J. Neuhauser, F. Ryter, J. Schweinzer, J. Stober, W. Suttrop, ASDEX Upgrade Team, and JET Team. Closed divertor operation in ASDEX Upgrade and JET. *Plasma Phys. Control. Fusion*, 41:B177, 1999.

[5] B. Lipschultz, B. LaBombard, J. L. Terry, C. Boswell, and I. H. Hutchinson. Divertor Physics Research on Alcator C-Mod. *Fusion Sci. Technol.*, 51:369–389, 2007.

[6] C. F. Sang, P. C. Stangeby, H. Y. Guo, A. W. Leonard, B. Covele, L. L. Lao, A. L. Moser, and D. M. Thomas. SOLPS modeling of the effect on plasma detachment of closing the lower divertor in DIII-D. *Plasma Phys. Control. Fusion*, 59:025009, 2017.

[7] H.Y. Guo, C.F. Sang, P.C. Stangeby, L.L. Lao, T.S. Taylor, and D.M. Thomas. Small angle slot divertor concept for long pulse advanced tokamaks. *Nuclear Fusion*, 57:044001, 2017.

[8] R. Schneider, X. Bonnin, K. Borrass, D.P. Coster, H. Kastelewicz, D. Reiter, V.A. Rozhansky, and B.J. Braams. Plasma Edge Physics with B2-Eirene. *Contrib. Plasma Phys.*, 46(1-2):3–191, 2006.

[9] A.S. Kukushkin, H.D. Pacher, V. Kotov, G.W. Pacher, and D. Reiter. Finalizing the ITER divertor design: The key role of SOLPS modeling. *Fusion Eng. Des.*, 86:2865, 2011.

[10] L.L. Lao, H.St. John, R.D. Stambaugh, A.G. Kellman, and W. Pfeiffer. Reconstruction of current profile parameters and plasma shapes in tokamaks. *Nuclear Fusion*, 25:1611–1622, 1985.

[11] Y. Feng, H. Frerichs, M. Kobayashi, A. Bader, F. Effenberg, D. Harting, H. Hoelbe, J. Huang, G. Kawamura, J. D. Lore, T. Lunt, D. Reiter, O. Schmitz, and D. Sharma. Recent Improvements in the EMC3-Eirene Code. *Contrib. Plasma Phys.*, 54(4-6):426–431, 2014.

[12] Y. Feng, F. Sardei, and J. Kisslinger. 3D fluid modelling of the edge plasma by means of a Monte Carlo technique. *Journal of Nuclear Materials*, 266-269:812–818, 1999.

[13] J.M. Canik, A.R. Briesemeister, C.J. Lasnier, A.W. Leonard, J.D. Lore, A.G. McLean, and J.G. Watkins. Modeling of detachment experiments at DIII-D. *Journal of Nuclear Materials*, 463:569 – 572, 2015. PLASMA-SURFACE {INTERACTIONS} 21Proceedings of the 21st International Conference on Plasma-Surface Interactions in Controlled Fusion Devices Kanazawa, Japan May 26-30, 2014.

[14] H. Frerichs, D. Reiter, O. Schmitz, D. Harting, T. E. Evans, and Y. Feng. On gas flow effects in 3D edge transport simulations for DIII-D plasmas with resonant magnetic perturbations. *Nuclear Fusion*, 52:054008, 2012.

[15] H. Y. Guo, D. N. Hill, A. W. Leonard, S. L. Allen, P. C. Stangeby, D. Thomas, E. A. Unterberg, T. Abrams, J. Boedo, A. R. Briesemeister, D. Buchenauer, I. Bykov, J. M. Canik, C. Chrobak, B. Covele, R. Ding, R. Doerner, D. Donovan, H. Du, D. Elder, D. Eldon, A. Lasa, M. Groth, J. Guterl, A. Jarvinen, E. Hinson, E. Kolemen, C. J. Lasnier, J. Lore, M. A. Makowski, A. McLean, B. Meyer, A. L. Moser, R. Nygren, L. Owen, T. W. Petrie, G. D. Porter, T. D. Rognlien, D. Rudakov, C. F. Sang, C. Samuell, H. Si, O. Schmitz, A. Sontag, V. Soukhanovskii, W. Wampler, H. Wang, and J. G. Watkins. Developing and validating advanced divertor solutions on DIII-D for next-step fusion devices. *Nuclear Fusion*, 56:126010, 2016.